



An asymmetric rainfall response to ENSO in East Asia

Ching Ho Justin Ng¹ · Gabriel A. Vecchi^{1,2,3} · Ángel G. Muñoz^{1,4} · Hiroyuki Murakami^{1,5}

Received: 17 November 2017 / Accepted: 7 May 2018 / Published online: 12 May 2018
© Springer-Verlag GmbH Germany, part of Springer Nature 2018

Abstract

This study explores the impact of El Niño and La Niña events on precipitation and circulation in East Asia. The results are based on statistical analysis of various observational datasets and Geophysical Fluid Dynamics Laboratory's (GFDL's) global climate model experiments. Multiple observational datasets and certain models show that in the southeastern coast of China, precipitation exhibits a nonlinear response to Central Pacific sea surface temperature anomalies during boreal deep fall/early winter. Higher mean rainfall is observed during both El Niño and La Niña events compared to the ENSO-Neutral phase, by an amount of approximately 0.4–0.5 mm/day on average per °C change. We argue that, in October to December, while the precipitation increases during El Niño are the result of anomalous onshore moisture fluxes, those during La Niña are driven by the persistence of terrestrial moisture anomalies resulting from earlier excess rainfall in this region. This is consistent with the nonlinear extreme rainfall behavior in coastal southeastern China, which increases during both ENSO phases and becomes more severe during El Niño than La Niña events.

1 Introduction

The El Niño-Southern Oscillation (ENSO) phenomenon, involving interannual variability in sea-surface temperatures (SST) in the equatorial Central/East Pacific and associated atmospheric changes, has significant influences on the global climate system (Ropelewski and Halpert 1987; Kane 1997), and has been shown to influence the probability of drought and flood events in many locations (Barlow et al. 2001; Tong et al. 2006). There have been a broad range of studies on the climatic impacts of ENSO (e.g., see Zebiak et al. 2015). Understanding the mechanisms connecting ENSO to

rainfall variability in East Asia is of scientific interest, and the potential impact of this understanding on improved seasonal forecasts for precipitation and its extremes underlines its societal significance. With these broad motivations, this study analyzes the influence of ENSO on seasonal rainfall and rainfall extremes, with particular focus on the East Asian subcontinent.

Many studies about ENSO teleconnections and their impacts on climate have been based on the assumption of linearity: that to a first approximation the impacts during El Niño largely mirror those during La Niña. This linear assumption has proved to be sufficient in explaining many aspects of ENSO and its teleconnections (Lau and Nath 2001; Alexander et al. 2002). However, differences in patterns, amplitudes and predictability between the El Niño and La Niña phases, which are often referred to as the asymmetry/nonlinearity of ENSO, have also been shown to exist in specific regions and seasons (Hoerling et al. 1997; Larkin and Harrison 2002; Jin et al. 2003; Choi et al. 2013; Dommenget et al. 2013). Hoerling et al. (1997) and Zhang et al. (2014) showed that surface temperature increases during both El Niño and La Niña in parts of North America. Larkin and Harrison (2002) described differences in atmospheric and oceanic patterns between El Niño composites and those of La Niña $\times (-1)$, such that these two phases are not simply opposite to each other. An and Jin (2004) described the asymmetry of El Niño events being stronger than La

✉ Ching Ho Justin Ng
chjng@princeton.edu

¹ Atmospheric and Oceanic Sciences (AOS), Princeton University, 300 Forrester Road, Sayre Hall, Princeton, NJ 08540-6659, USA

² Department of Geosciences, Princeton University, Princeton, NJ 08540-6649, USA

³ Princeton Environmental Institute, Princeton University, Princeton, NJ 08540-6649, USA

⁴ International Research Institute for Climate and Society (IRI), The Earth Institute, Columbia University, Palisades, NY 10964-1000, USA

⁵ NOAA/Geophysical Fluid Dynamics Laboratory, Princeton University, Princeton, NJ 08540-6649, USA

Niña as an intrinsic nonlinear characteristic of ENSO, while Ohba and Ueda (2009) described nonlinear wind response from forcing an atmospheric model with antisymmetrical SST anomalies. Vecchi and Harrison (2006), Vecchi (2006) and Lengaigne and Vecchi (2010) emphasized the importance of the nonlinear equatorial zonal wind and convection response to SST in extreme El Niño events, and proposed mechanisms leading to this nonlinearity. Hong et al. (2010) described a larger amplitude of warming in the Indian Ocean during El Niño than that of cooling during La Niña, and suggested mechanisms leading to this. More recently, Dommenget et al. (2013) and Choi et al. (2015) further described nonlinearity of the zonal wind response to ENSO in Central Pacific. The asymmetry in atmospheric circulation responses to ENSO is also used in Cai et al. (2015) to understand a robust response of ENSO precipitation to atmospheric global warming, and in Li et al. (2016) to describe asymmetry in Northeast Asia vegetation cover.

In this study, we aim to gain an understanding of the precipitation response to ENSO in East Asia during the fall/winter season, which is generally the most mature period of El Niño (Rasmusson and Carpenter 1982), by analyzing precipitation behavior from several observational datasets and numerical models. We begin by assessing the assumption of linearity for ENSO climatic impacts, and performed a linear regression for the rainfall-SST relationship to examine any linear response to ENSO, with respect to the Neutral-climatological rainfall as shown in Fig. 1; details about datasets and methodology used are documented in Sect. 2. This linear regression (Fig. 2) shows that in boreal deep fall/early winter, a clear linear signal is seen in the maritime continent and Central China, consistent with Larkin and Harrison (2005). The linear

signal is however absent, for example, along the southeastern coast of China (hereafter SEC) and particularly in the OND season.

The result that the relationship is not linear in many regions is worth further investigation. In particular, we may intuitively expect that ENSO would impact precipitation in SEC because of its proximity to the Pacific and the existence of El Niño teleconnections in this region (Zhang et al. 1999; Wang et al. 2000; Zhang and Sumi 2002; Wu et al. 2003). Past literature has reported positive rainfall anomalies in southern China during fall/winter El Niño events, resulting from an anomalous anticyclone to the north of the maritime continent which drives anomalous onshore southwesterly moisture fluxes in the SEC. However, the nonlinear nature of the SEC rainfall response to ENSO has not been previously described. Since the regression suggests that a linear relationship does not hold in SEC, would there exist a ‘nonlinear’ signal, in the sense that rainfall increases or decreases during both El Niño and La Niña? To examine the possible ‘nonlinearity’ in SEC, we performed a ‘quasi-linear’ model fit to the data (see Sect. 2.3). This analysis demonstrates that a nonlinear response of rainfall to ENSO is indeed observed in SEC during deep fall/early winter, particularly the OND season.

This paper is structured as follows. Section 2 introduces the datasets and models studied, in addition to the methodology to examine ‘nonlinearity’. This is followed by a description of the nonlinear rainfall response in Sects. 3, and 4 discusses the possible mechanisms for this response. Section 5 presents the implications of this nonlinearity on extreme rainfall, while the final section provides some concluding remarks.

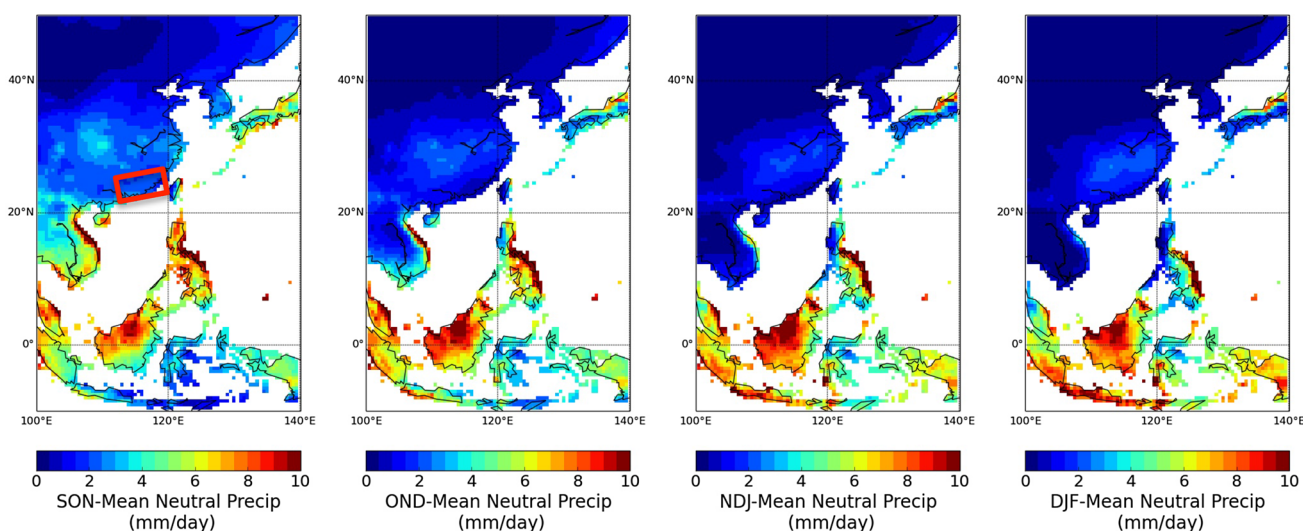


Fig. 1 Observed climatological rainfall, during the ENSO-Neutral phase, from APHRODITE in East Asia in the fall/winter season. The red box represents the general location of ‘the southeastern coast of China (SEC)’ discussed in the text

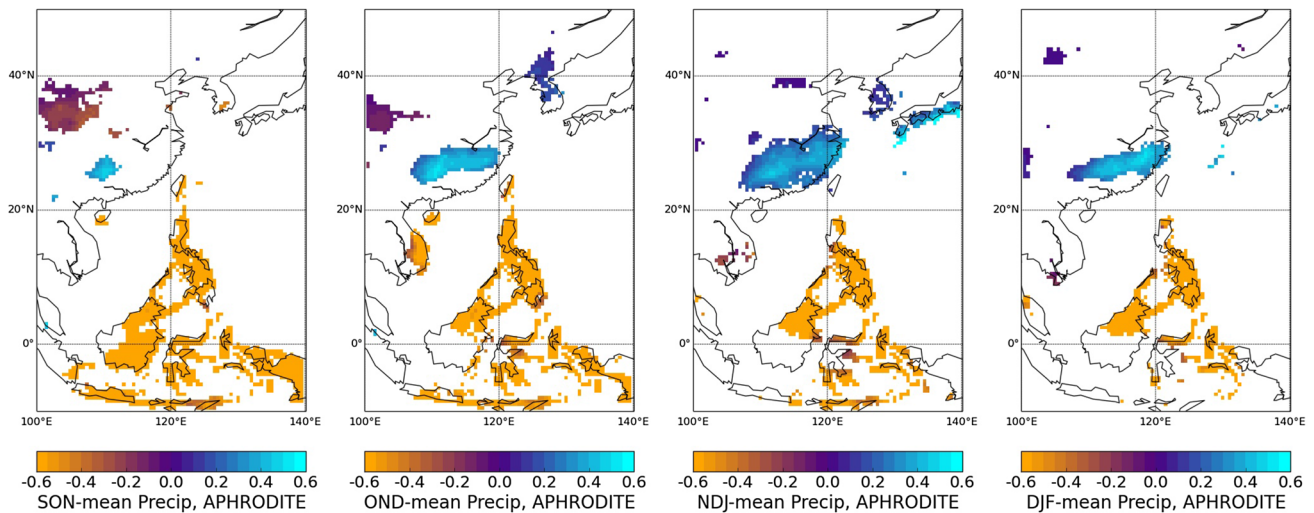


Fig. 2 Linearity of rainfall response to ENSO, given by the rate of increase of APHRODITE seasonal-mean rainfall against Niño-3.4 Index (mm/day/°C). This is defined by the slope of linear (median of

pairwise slopes) regression of seasonal-mean rainfall against Niño-3.4 Index. Only locations whose anomalies are statistically significant at the one-sided 99% level are plotted

2 Data and methodology

The response of rainfall to ENSO is analyzed using a suite of observational datasets along with coupled global climate model simulations. A quasi-linear regression of SST and rainfall is used to determine the extent of nonlinearity in the rainfall-ENSO relationship. This section describes the observational datasets and numerical models studied, and the methodology to quantify the ‘nonlinearity’ of rainfall response.

2.1 Rainfall observational datasets

We begin our analysis of rainfall response to ENSO with the Japan-initiated data assimilation project named Asian Precipitation—Highly-Resolved Observational Data Integration Towards Evaluation (APHRODITE, Yatagai et al. 2009, 2012). APHRODITE is a recently published land-based observational network comprised of rain gauge data from various Asian countries and regions. We studied the APHRODITE Monsoon Asia Version 11.01 data product (APHRO_MA_V1101), for the 50-year period between 1958 and 2007. Daily high-resolution rainfall values are provided, in addition to the ‘rstm’ index which describes the density of observation stations within each grid cell. This study focuses on the East Asian region bounded within 50°N–10°S, 100°E–140°E (Fig. 1), with resolution of 0.5° × 0.5°.

Throughout this study, Version 4 of the Extended Reconstructed Sea Surface Temperature dataset (ERSSTv4, Smith et al. 2008) is used for the Niño-3.4 Index (averaged SST within 5°N–5°S, 120°W–170°W). El Niño and La Niña events are defined with a threshold of ± 0.5 °C for the

3-month running mean of ERSSTv4 SST anomalies in the Niño-3.4 region, also known as the Oceanic Niño Index, based on centered 30-year base periods (see website: http://www.cpc.ncep.noaa.gov/products/analysis_monitoring/ensostuff/ensoyears.shtml).

To place the results using APHRODITE in a broader context, we also analyzed a number of other precipitation datasets:

- NOAA PREC/L (Precipitation Reconstruction Over Land): Monthly precipitation values for land, 1950–2011, resolution 0.5° × 0.5° (Chen et al. 2002), created by gridding data from over 17,000 gauge observations in the Global Historical Climatology Network (GHCN) and the Climate Anomaly Monitoring System (CAMS) datasets using the optimal interpolation scheme;
- GPCP (Global Precipitation Climatology Project), Version 2.2: Monthly values for land and ocean, 1979–2014, resolution 2.5° × 2.5° (Adler et al. 2003), a merged analysis product incorporating precipitation estimates from surface rain gauge observations, satellite microwave and infrared data;
- CMAP (CPC Merged Analysis of Precipitation): Monthly values for land and ocean, 1979–2014, resolution 2.5° × 2.5° (Xie and Arkin 1997), also created by merging gauge observations with satellite estimations, in addition to the NCEP-NCAR reanalysis;
- University of Delaware Air Temperature and Precipitation Dataset, Version 4.01: Monthly values for land, 1950–2014, resolution 0.5° × 0.5° (Willmott and Matsuura 2001), gridded from land gauge observations using the Shepard interpolation algorithm.

2.2 Numerical models

To assist in interpreting the ENSO response of precipitation in observational datasets, a suite of model simulations from GFDL's coupled global climate models are studied: The Climate Model Version 2.1 (CM2.1, Delworth et al. 2006), the Forecast-Oriented Low Ocean Resolution Version of Climate Model Version 2.5 (CM2.5-FLOR, hereafter FLOR), and the Low Atmosphere and Ocean Resolution Version of Climate Model Version 2.5 (CM2.5-LOAR, hereafter LOAR). FLOR consists of the atmosphere and land components of CM2.5 (Delworth et al. 2012) coupled with the ocean and sea ice components of the lower-resolution CM2.1. The atmosphere and land components of FLOR have a horizontal resolution of $0.5^\circ \times 0.5^\circ$ (approximately $50 \text{ km} \times 50 \text{ km}$), while the ocean and sea ice components have a horizontal resolution of $1^\circ \times 1^\circ$ (telescoping to $1/3^\circ$ meridional spacing near the Equator). LOAR shares the same model components and physical parameterizations as FLOR, except that the atmosphere and land components have a lower horizontal resolution of $2^\circ \times 2^\circ$ (C48 grid, as opposed to C180 in FLOR). More details on the FLOR model setup can be found in Vecchi et al. (2014), and those for LOAR in van der Wiel et al. (2016).

We analyzed a series of nudged-SST simulations with the models, which artificially require the models to closely follow observed sea-surface temperatures by restoring model SSTs to the interannually varying monthly-mean observed value (SST_{Obs}) from the Met Office Hadley Centre Sea Ice and SST dataset (HadISST1.1, Rayner et al. 2003), such that the model SST satisfies $\partial_t SST = \overline{SST} + (SST_{Obs} - SST)/\tau$, where $\partial_t SST$ represents the partial time-derivative of the SST field, \overline{SST} represents the SST tendency as computed in the coupled model, and τ is the restoring timescale. Ten ensemble members are used for CM2.1 (study period: 1971–2010), all of which perform monthly SST nudging with 5-day restoring timescales (Fanrong Zeng, personal communication). Five ensemble members are used for LOAR (study period: 1980–2009), all of which perform monthly SST nudging with 5-day restoring timescales (Muñoz et al. 2017). Nudged-SST simulations of FLOR (study period: 1971–2010) have six ensemble members with 5-day or 10-day restoring timescales (Murakami et al. 2015). Following Murakami et al. (2015), since the difference in rainfall simulation between these restoring timescales is small (not shown), we treat both types equally to give six ensemble simulations for FLOR. Throughout this paper, we will consider ensemble-mean results for the simulations.

In models, El Niño and La Niña events are defined in the same way as for observations. Since model SSTs are nudged to observations, ENSO events occur in the same years as in observations.

2.3 Diagnosis of nonlinearity

Beginning with the assumption of linearity to examine the rainfall response to ENSO, for each running 3-month season, we performed a linear regression of the seasonal-mean APHRODITE precipitation (for each grid cell in East Asia) to the average Niño-3.4 Index in that season, for a total of 50 years between 1958 and 2007. In particular, following Lanzante (1996), we performed a median of pairwise slopes fit, which is shown to be reasonably efficient for a sample size of 50. The results of this regression have been shown in Fig. 2, and will be discussed in more detail in the next section.

As briefly mentioned in the introduction, the inadequacy of a linear model in our region of interest implies the need to consider nonlinear impacts of ENSO on climate. For this purpose, we fit a 'quasi-linear' function for seasonal-mean APHRODITE rainfall (y) against the mean Niño-3.4 Index in that season, up to de-averaging with the 50-year mean Index (i.e. $x := x - \bar{x}$, where x is the seasonal Niño-3.4 Index, and $\bar{\cdot}$ represents the 50-year mean), for the 50 years between 1958 and 2007. The 'quasi-linear' function takes the form $y = a|x| + bx + c$, where y is precipitation, x is the Niño-3.4 Index, and coefficients a , b , c are to be determined. This is a single n-linear function, and it enables us to calculate a non-dimensional 'linearity ratio' defined as $L = \log(|b|/|a|)$, which provides a measure of the nonlinearity of the rainfall response. To see this, consider the case where L becomes increasingly positive, for which $|b| \gg |a|$, and hence y behaves like the linear function $bx + c$, giving a close-to-linear relationship (rainfall increase in one phase and decreases in the other). In contrast, when L becomes increasingly negative, then $|b| \ll |a|$, giving $y \sim a|x| + c$ and the relationship is substantially v-shaped. L close to zero indicates a one-sided response, i.e. there is no rainfall response to ENSO during either the El Niño or La Niña phase.

While the ratio L is useful to describe the character and linearity of the rainfall-SST relationship, it does not provide information about the phasing of the response within each category. For a linear relationship, a positive value of L describes both positively linear ($y \sim bx$, $b > 0$) and negatively linear ($y \sim bx$, $b < 0$) relationships. When L is negative, the relationship can be positively ($y \sim a|x|$, $a > 0$) or negatively ($y \sim a|x|$, $a < 0$) v-shaped, so that rainfall either increases or decreases in both phases. When L is close to zero, the one-sided rainfall response can be positive or negative in either phase.

The magnitude of the rainfall response in each category is implied by the values of coefficients a , b . In the limiting case where there is no relationship between rainfall and ENSO ($y = \text{constant}$), L is not well defined and can take any value as the coefficients a , b tend to zero.

3 Results

Our analysis of observational datasets reveals that a relationship between rainfall and ENSO exists in various places in the Eastern Hemisphere, but it is not ubiquitously linear as we might expect from the perception that El Niño is opposite to La Niña. Along the southeastern coast of China, higher rainfall is observed in both El Niño and La Niña than ENSO-Neutral during the OND season.

3.1 Signal-to-noise ratio

While the linear regression or the quasi-linear function described in Sect. 2.3 can be used to correlate rainfall to Niño-3.4 SST for each grid cell in East Asia, it makes sense to only focus on regions with a clear enough signal. For this purpose, we define the signal-to-noise (STN) ratio, as the variance of the (linear or quasi-linear) model-predicted rainfall over the 50-year period, divided by the variance of the residual (model-prediction minus observation) over the same period. A bootstrap test (Efron and Tibshirani 1985, with 1000 bootstrap samples) is performed for the signal-to-noise ratio in each grid cell, and hereafter we will focus our attention on locations with statistically significant anomalies at the one-sided 99% significance level.

3.2 Seasonal variability of relationship

We initiated our study of the rainfall response to ENSO based on a linear assumption and performed a linear

regression for the rainfall-SST relationship. Figure 2 shows that during the fall season, this linear relationship exists (statistically significant at the 99% level) in various regions of East Asia but is not ubiquitous.

Certain regions including the southeastern coast of China, for which ENSO teleconnections are suggested in the literature (see, for example, Zhang et al. 1999), do not exhibit a linear signal, particularly for the OND season. (While a linear signal emerges in the SEC region as winter progresses, we will show later that the responses are in fact closer to one-sided, noting that these responses may be captured by both linear and non-linear regressions; during OND, however, the linear signal completely vanishes.) Regions with an absence of a linear signal invite most attention, and the focus of this paper will be on examining the rainfall response to ENSO in the densely-populated SEC region.

While the linear regression shows otherwise, we intuitively expected a rainfall-SST relationship to exist in SEC, as mentioned in the introduction. Since a linear signal is not captured in the regression, this might imply the possibility of a nonlinear rainfall response to ENSO, where rainfall increases not only during the warm but also the cold phase.

To examine any nonlinearity in the rainfall response, we applied a quasi-linear fit to the rainfall-ENSO relationship, as described in Sect. 2.3 to compute the linearity ratio L for each grid cell and season (Fig. 3). When the linear assumption is forfeited, a clear (nonlinear) signal becomes evident along SEC during the OND season (which becomes closer to one-sided as winter progresses), and hence our focus on deep fall/early winter for SEC in this study. The nonlinear rainfall-ENSO in APHRODITE

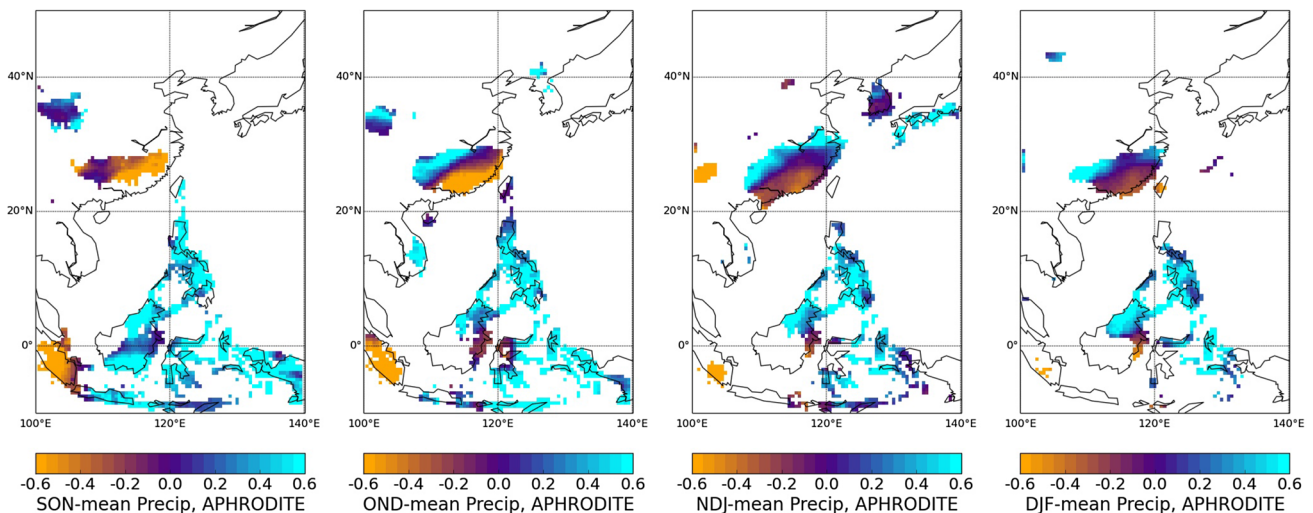


Fig. 3 Nonlinearity of rainfall response to ENSO, given by the linearity ratio L for APHRODITE seasonal-mean rainfall. Negative (positive) values of L indicate nonlinear (linear) rainfall responses to ENSO. Only locations whose anomalies are statistically significant at

the one-sided 99% level are plotted. Note the SEC region with shading over orange color (nonlinear response) in the OND season, which will be the focus of this paper. This region also exhibits a one-sided (purple) relationship in the later seasons

is statistically significant at the 99% level in this region, and the quasi-linear model substantially improves signal-to-noise ratio over the linear model (Fig. 4). For grid cells along the coast in the APHRODITE system with $L \leq -0.2$, the STN ratio often exceeds 50% during the OND season. It is worth noting that the SEC region is also one with moderately high observing station density used to build the APHRODITE dataset. The rainfall response to ENSO in the OND season is positively v-shaped: on average,

rainfall is higher during both El Niño and La Niña than ENSO-Neutral by approximately 0.4–0.5 mm/day per °C change in Niño-3.4 SST (Fig. 5). As winter progresses, the fitted quasi-linear function becomes one-sided, with rainfall increasing during El Niño and a small anomaly during La Niña, as seen by coefficients a, b both positive in the quasi-linear fit (not shown). The one-sided rainfall response in DJF is consistent with Guo et al. (2017).

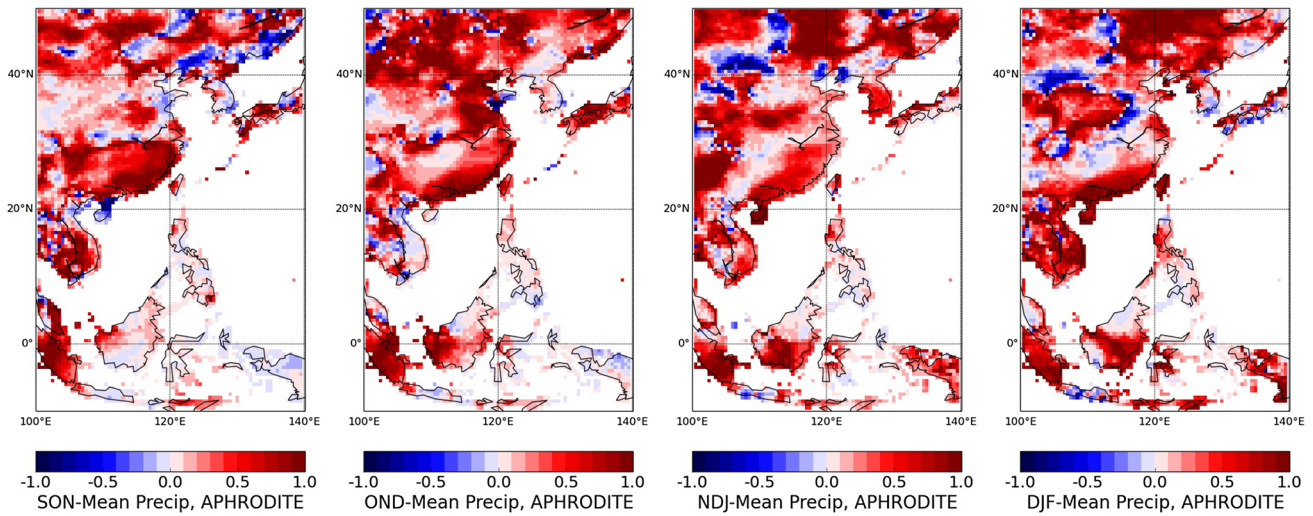


Fig. 4 Nonlinearity of rainfall response to ENSO, depicted by the proportional change of signal-to-noise ratio using quasi-linear model (Fig. 3) over linear model (median of pairwise slopes) (Fig. 2) in APHRODITE. Proportional change is defined as (Quasi-

linear STN – Linear STN)/(Quasi-linear STN+Linear STN), and is bounded between –1 and 1. Using quasi-linear model improves the signal-to-noise ratio in the SEC region

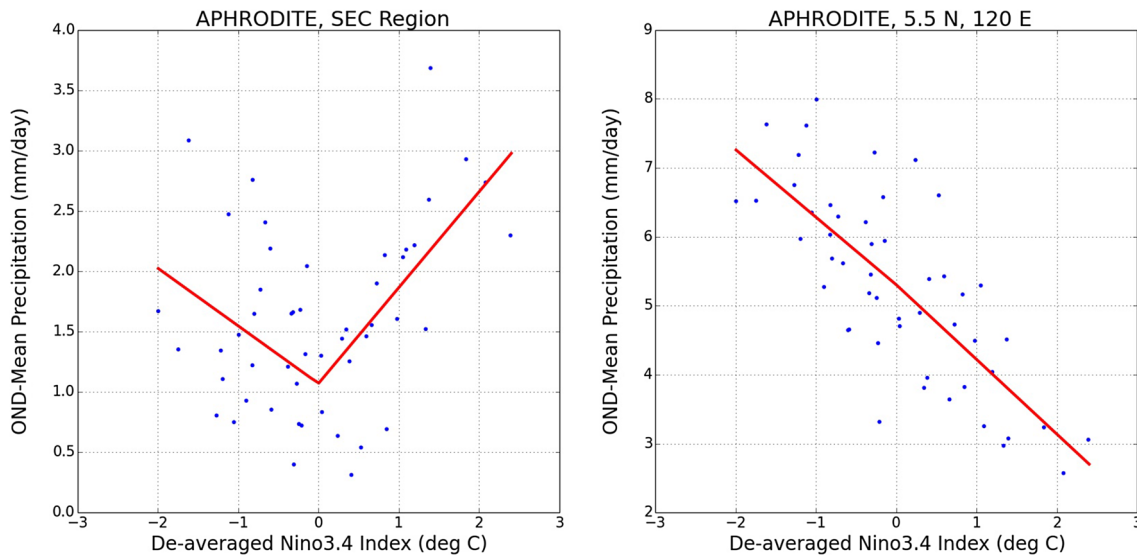


Fig. 5 Response to rainfall to ENSO, with OND-mean APHRODITE rainfall plotted against de-averaged Niño-3.4 Index, for (left) averaged locations in the SEC region (here defined as 23°N–27°N,

111°E–118°E), and (right) at 5.5°N, 120°E (Southern Philippines), plotted for comparison. The fitted quasi-linear function is given by the red line in each plot

3.3 Other datasets

The NOAA PREC/L rainfall dataset and the U. of Delaware Air Temperature & Precipitation Dataset show a nonlinear response in the SEC region during OND similar to that in APHRODITE (Fig. 6). The nonlinearity is less evident in the lower-resolution CMAP and GPCP datasets. Examination of the quasi-linear function coefficients shows that the relationship is positively v-shaped, as in APHRODITE, so that rainfall is higher in both El Niño and La Niña phases. In NOAA PREC/L, rainfall also increases at a rate of approximately 0.4 mm/day per °C change in Niño-3.4 SST. Notably, CMAP and GPCP date back to only 1979 while APHRODITE data between 1958 and 2007 was studied; in fact, if instead we focused on APHRODITE data between 1979 and 2007, a similar nonlinear response can also be observed (not shown).

3.4 Numerical models

We look to a suite of numerical model experiments as a way to understand the sources of the rainfall-ENSO nonlinearity in the SEC, taking advantage of a hierarchy of models in which some models show the nonlinearity and others do not. The most comprehensive model, FLOR, captures a nonlinear relationship of rainfall to ENSO during the OND season in its nudged-SST simulations, with a positively v-shaped signal in the SEC region (Fig. 7). Similar to APHRODITE, the response becomes closer to one-sided as winter progresses (Fig. 8). The rainfall-ENSO relationship in this model is statistically significant at the one-sided 99% level ($p < 0.01$). In LOAR and CM2.1, however, the SEC ENSO precipitation

signal remains noisy throughout all seasons. While the number of ensemble members of CM2.1 (ten) outnumber that in FLOR (six) and LOAR (five), similar results are obtained when five members from CM2.1 are considered; in particular, we note the incapability of CM2.1 to simulate realistic rainfall behavior, with its rainfall response to ENSO remaining statistically insignificant even when the ensemble-mean from ten members is evaluated.

The global coverage of the FLOR model with relatively high resolution enables us to extend our quasi-linear model methodology to regions outside of East Asia (Fig. 9). (Indeed, some of the observational datasets described in Sect. 2.1 also have global coverages, but GPCP and CMAP have lower resolutions, while the higher-resolution datasets are geographically limited to land surfaces.) Figure 9 shows that the nonlinearity of the rainfall response to ENSO is not limited to the SEC region, but also exists in the tropical Eastern Pacific and Central Australia. In particular, the nonlinear (one-sided) response in Eastern Pacific is consistent with Vecchi (2006) and Lengaigne and Vecchi (2010), in which they suggested the (one-sided) nonlinearity in Eastern Pacific is contributed by the onset of deep convection in this region during extreme El Niño events. On the other hand, the rainfall nonlinearity in Central Pacific has been described in Zhang et al. (2014), and suggested to be a driver of a series of ENSO asymmetries, including the nonlinear equatorial zonal wind response to ENSO (Dommenget et al. 2013; Choi et al. 2013, 2015). Given the statistical significance of nonlinear anomalies in the SEC region and the comparative scarcity of rainfall accounts in East Asia, we have focused on the densely-populated SEC region in this study, and will

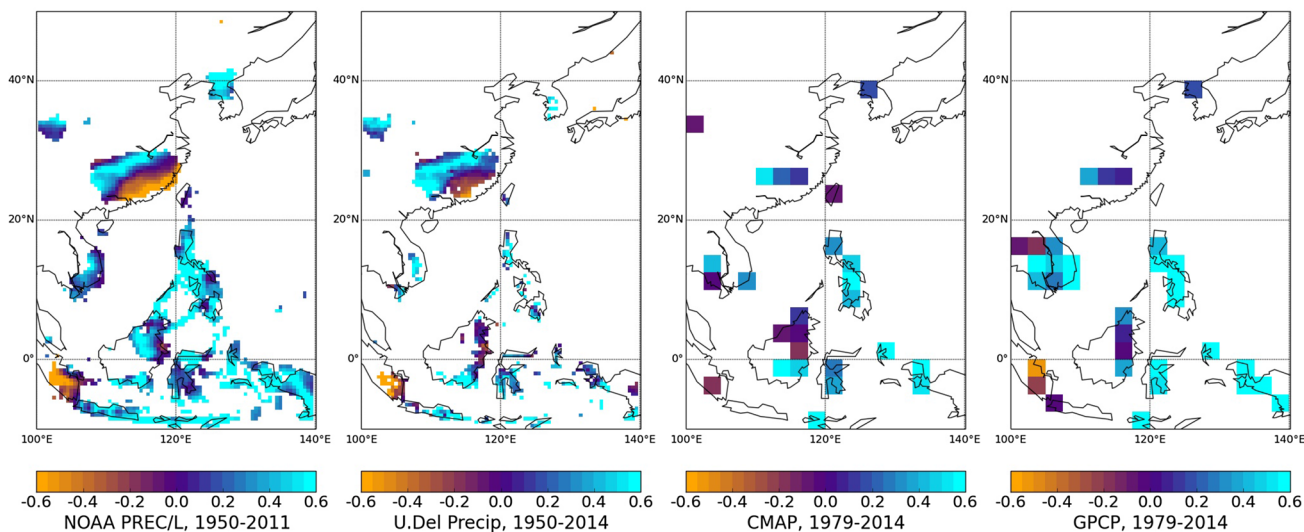


Fig. 6 Nonlinearity of OND-mean rainfall response to ENSO, in (left to right) NOAA PREC/L, U. of Delaware Air Temperature and Precipitation Dataset, CMAP and GPCP, as given by the linearity ratio

L. Only locations whose anomalies are statistically significant at the one-sided 99% level are plotted

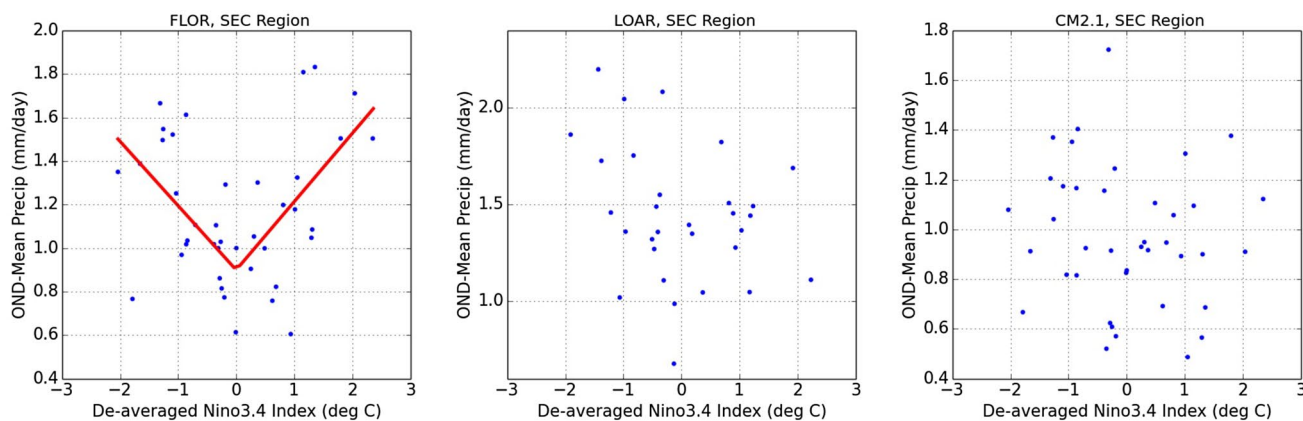


Fig. 7 Rainfall response to ENSO in numerical models. In FLOR (left), OND-mean rainfall is higher during both El Niño and La Niña phases than ENSO-Neutral in the SEC region (23°N–27°N, 111°E–118°E). The fitted quasi-linear function is given by the red line. The rainfall response signal in this region is noisier in LOAR (middle) and CM2.1 (right) than in FLOR

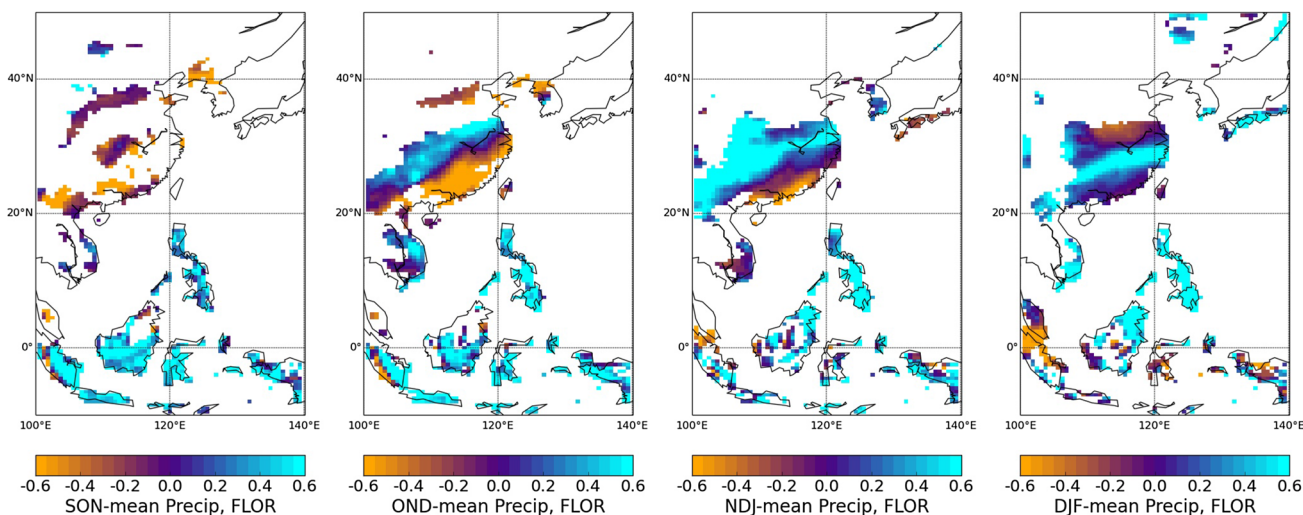


Fig. 8 Nonlinearity of rainfall response to ENSO in FLOR nudged-SST simulations, given by the value of linearity ratio L . Only locations whose anomalies are statistically significant at the one-sided 99% level are plotted

discuss about possible mechanisms leading to this nonlinearity, together with its implications on extreme rainfall, in the next sections.

4 Mechanisms behind the nonlinearity

We have so far presented the diagnosis of the existence of a nonlinear rainfall response to ENSO in the southeastern coast of China, in which the mean and extreme rainfall increases during both El Niño and La Niña during the OND season. This nonlinearity is captured in multiple observational datasets and FLOR nudged-SST simulations, but not in LOAR and CM2.1. In this final section, we now briefly

discuss possible mechanisms to explain the nonlinear rainfall response in the SEC region.

The increased rainfall during El Niño has been previously explained by Zhang et al. (1999) and Wang et al. (2000), in which they suggested that an anomalous high pressure to the north of the maritime continent results in anomalous onshore southwesterlies in southern China during fall/winter seasons, and hence enhanced rainfall in this region. In this study, evidence from the FLOR model regarding the large-scale circulation anomalies (Fig. 10) is found to be consistent with existing literature. In particular, the anomalous onshore southwesterlies captured in FLOR during El Niño result in anomalous moisture fluxes ($P-E$) into the SEC region (Fig. 11a), and remains so for the entire fall/winter season. In LOAR and CM2.1, however, this anomalous high

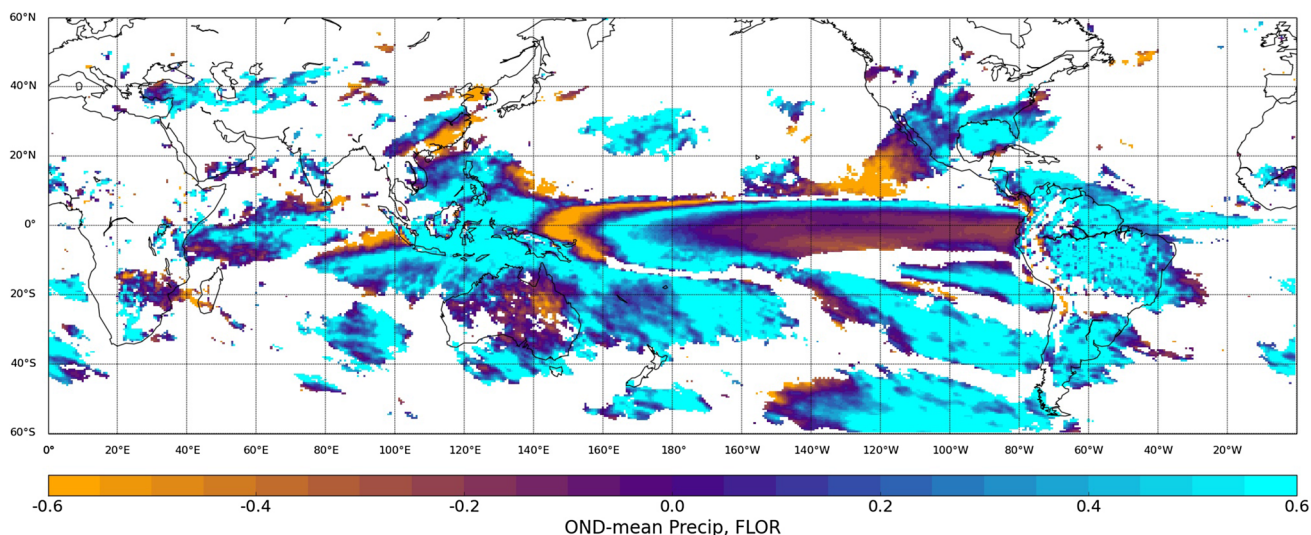


Fig. 9 As in Fig. 8, for OND-mean rainfall, plotted between 60°N–60°S

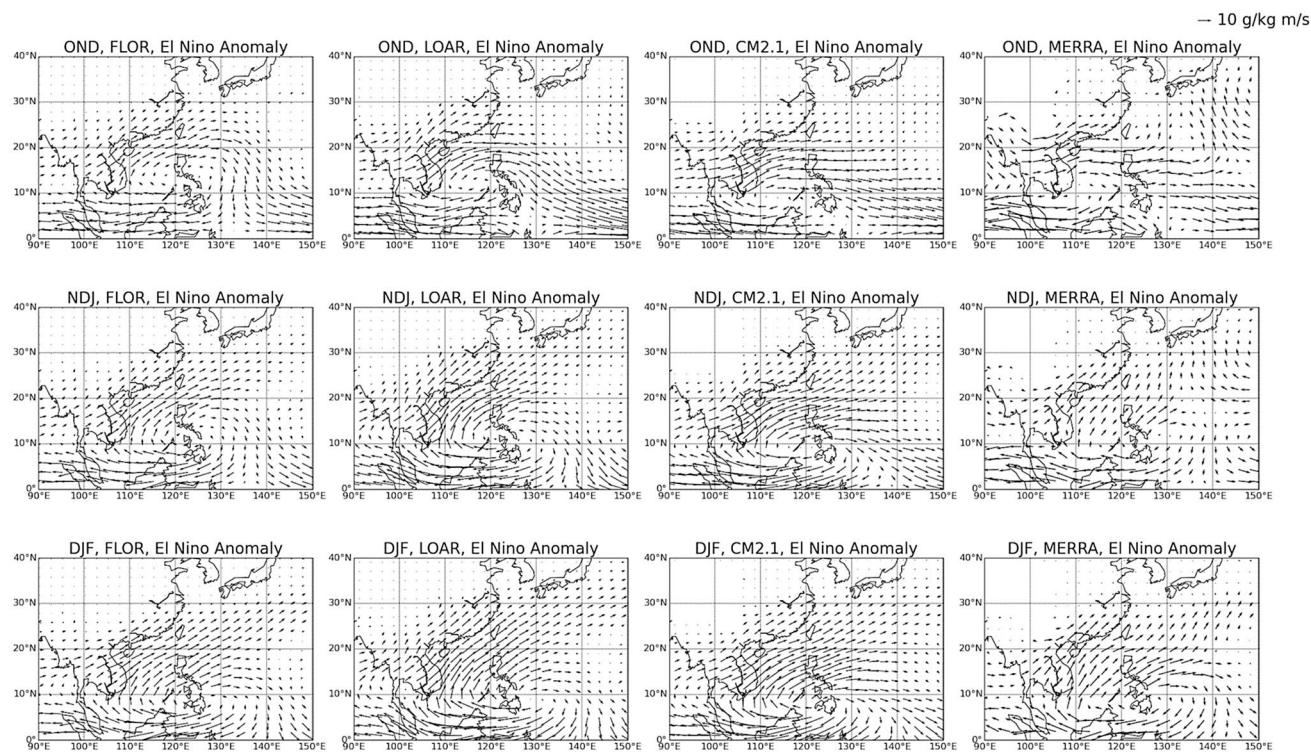


Fig. 10 Composites of 850 hPa moisture flux anomalies during El Niño, in (left to right) FLOR, LOAR, CM2.1 and MERRA. Specific humidity and wind variables from MERRA are taken from the 3-h Assimilated Meteorological Fields simulation with 1.25°×1.25° horizontal resolution, for 1979–2014. During the OND season, FLOR exhibits an anomalous anticyclonic circulation near the maritime

continent, which is displaced westward in LOAR and CM2.1. The moisture flux anomalies in MERRA (1979–2014) are also shown for comparison purposes; while we have discussed the moisture budget in the models, we have not done so for reanalysis products, since the evaporative flux exhibits a negligible response to El Niño in MERRA (not shown)

is displaced westward during the OND season, so that the anomalous southwesterlies have a smaller onshore component (Fig. 10), giving a smaller El Niño rainfall anomaly

(and a noisier signal). After OND, anomalous flow has a higher onshore component so the rainfall anomaly becomes more positive (Fig. 11b, c), as is FLOR.

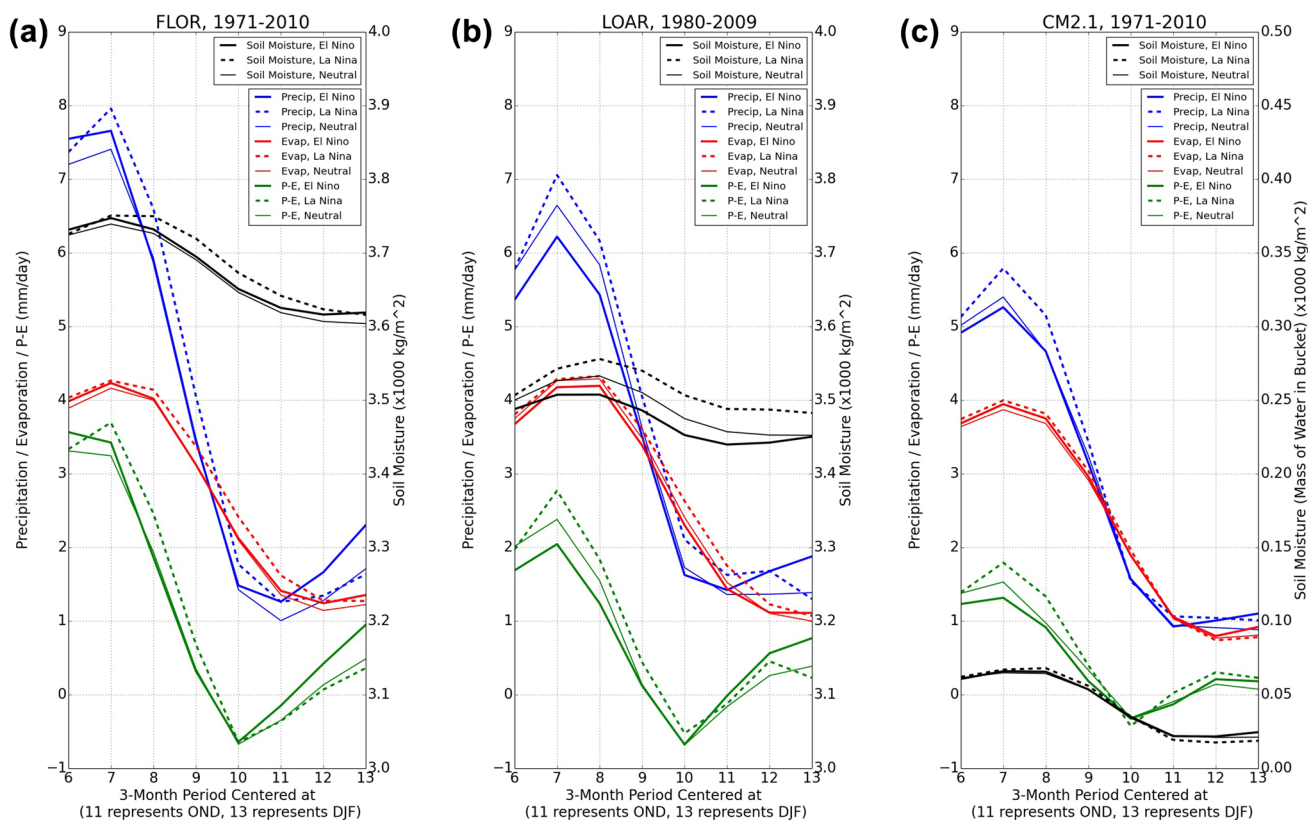


Fig. 11 Time evolution of precipitation (blue), evaporation (red), P–E (green) and soil moisture (black) in **a** FLOR, **b** LOAR and **c** CM2.1, averaged over the SEC region (23°N – 27°N , 111°E – 118°E). Note the different scales for soil moisture across the models

An analysis of the moisture budget through the relative contributions of precipitation, evaporation (local source of moisture), and their residual (non-local source, moisture fluxes), suggests that the weaker onshore southwesterly winds during El Niño, in the OND season, gives a smaller moisture flux convergence over the SEC region in LOAR (0.148 mm/day) and CM2.1 (-0.036 mm/day) than FLOR (0.200 mm/day). The moisture budget is computed as such due to the lack of high-frequency three-dimensional atmospheric moisture and wind model data, and since the convergence of time-averaged, column-integrated moisture flux in the atmosphere must be balanced by the excess of precipitation over evaporation (Seager and Vecchi 2010; Baldwin and Vecchi 2016). During DJF, the moisture flux convergence over SEC is positive in all models (FLOR: 0.463 mm/day , LOAR: 0.381 mm/day , CM2.1: 0.107 mm/day).

It is worthwhile to note that the ENSO SST anomaly pattern is similar between the models, since the sea-surface temperatures in these simulations are nudged to the same HadISST observational target. Since the oceanic controls are forced to be very similar, and since both FLOR and LOAR are inherited from the same parent model GFDL-CM2.5, we hypothesize that the different atmospheric circulation responses to ENSO, including the shift in the position of the

anomalous high pressure during El Niño, is largely due to the difference in horizontal resolutions in the atmospheric model component. The association between decreased model resolution and the shift of atmospheric circulation involves detailed investigation into the parameterizations of each model component and likely a large suite of additional experiments, which we will not explore in full detail in this paper.

While OND precipitation increases arise from the simultaneous atmospheric conditions during El Niño, we hypothesize that the anomalous rainfall during La Niña is the result of temporally nonlocal (lagged) moisture availability, so that past net precipitation increases are maintained in soil moisture to become available to the land-atmospheric state over the SEC region in OND. In both LOAR and FLOR models, precipitation exceeds evaporation ($P-E > 0$) in the ENSO-Neutral climatology during the summer season (Fig. 11a, b), resulting in excess surface water over the SEC region. Due to anomalous onshore southwesterlies during La Niña (not shown), excess P–E has a positive anomaly. Additionally, the time evolution of precipitation and evaporation suggests that mean P–E switches from positive to negative during Neutral and La Niña in the SON/OND season. The combined effect is that during the ENSO-Neutral phase, surface water

is in excess during summer, persists into SON/OND and then re-evaporates; when La Niña occurs, the positive P–E anomaly implies the existence of anomalous excess of surface water from summer, which also persists into the SON/OND season, providing a source for excess re-evaporation and leading to higher precipitation and evaporation rates. Indeed, there is anomalous soil moisture in both LOAR and FLOR models during La Niña across the SON/OND season, so that both models are able to capture this recirculation/recycling effect. While seasonal-mean values of precipitation and evaporation are being considered here, soil moisture is calculated from monthly instantaneous values (at the end of each month), and is integrated over the entire soil thickness, since monthly-mean values of top-layer soil moisture is unavailable from the models. We have made the additional assumption that soil moisture anomalies are due to anomalies in the top layer, while soil layers below are relatively static. While there is also anomalous La Niña P–E during the summer months in CM2.1, the moisture recycling effect is not captured in this model (Fig. 11c), hence not giving the nonlinear rainfall response—the implications of which will be discussed in later text.

From the moisture budget analysis viewpoint, the anomalous La Niña values of precipitation and evaporation in the OND season are 0.254 (0.265) mm/day and 0.265 (0.227) mm/day respectively in FLOR (LOAR), while the simultaneous moisture flux convergence (diagnosed from P–E) takes a small value of -0.011 (0.039) mm/day in FLOR (LOAR). The anomalous La Niña P–E in the preceding season is 0.522 (0.290) mm/day in FLOR (LOAR), part of which persists to OND and supports the anomalous evaporation rates in this season. Since the anomalous precipitation rate is very similar to that of evaporation in FLOR and LOAR during La Niña in OND, there is no room for non-local moisture fluxes to contribute to rainfall. In CM2.1, the anomalous La Niña moisture flux convergence over SEC region reads 0.117 mm/day, and the moisture recycling effect is not captured.

While the recycling effect is evident during La Niña only in FLOR and LOAR (but not in CM2.1), this effect does not appear dominant during El Niño since there is no anomalous P–E during summer, so that rainfall increases only as a result of anomalous onshore moisture fluxes, as outlined above. Therefore, during the OND season, the moisture recycling effect during La Niña and anomalous onshore fluxes during El Niño in FLOR (but not LOAR) are responsible for the nonlinear (positively v-shaped) rainfall response in FLOR.

As winter progresses, P–E once again becomes positive, so that the moisture recycling effect from previous excess surface water vanishes. Meanwhile, there exist anomalous northeasterly (offshore) fluxes as a result of strengthened East Asian Winter Monsoons (Wang et al. 2000) during La Niña in FLOR (Fig. 12), giving no anomalous moisture flux into the SEC region, as seen by the anomalous P–E being

close to zero (or slightly negative) in this model. Together with anomalous southwesterly flow (increased rainfall) during El Niño, the rainfall signal is closer to one-sided in FLOR. The rainfall signal is not statistically significant in the other two models.

This hypothesis emphasizes the importance to simulating and predicting rainfall anomalies in East Asia of enhanced horizontal resolution in the atmospheric model, and that an improvement of the land model is also critical in capturing rainfall contribution from land–atmosphere interactions. In particular, the recycling effect during La Niña is captured in both the FLOR and LOAR models (both of which are coupled with the LM3 land model), but is not captured in CM2.1, which has a less sophisticated land component (LM2). Additionally, the rainfall response signal in LOAR and CM2.1 (as given by fitting the quasi-linear function) is not statistically significant in the OND season (Fig. 7), which we hypothesize to be due to a westward displacement of the anomalous high pressure during El Niño. In fact, we interpret Fig. 7 as evidence that the improvement in simulating El Niño rainfall in FLOR than the other two models is driven more by an improvement in the response of its circulation to El Niño than that in the climatological mean state. Based on this hierarchy of models, we suggest that FLOR is able to capture both the El Niño moisture flux effect and La Niña recycling effect with its high atmospheric resolution and more sophisticated land component, respectively. LOAR, with its lower atmospheric resolution combined with the LM3 land component, only captures the La Niña recycling effect, while the LM2 component of CM2.1 renders its incapability to capture the La Niña recycling effect either. This hierarchy indicates that the nonlinear impacts of ENSO on rainfall are established not only through the atmosphere component of the climate system, but also its interaction with land hydrology.

5 Implications on extreme rainfall

The distinct mechanisms for the El Niño and La Niña responses bear on extreme rainfall behavior during the fall season. The different processes influencing rainfall during El Niño and La Niña modify the precipitation distribution in various ways. During El Niño, extreme rainfall becomes stronger, since anomalous moisture fluxes have the potential to create extreme rainfall, so that the mean rainfall anomaly is also driven by anomalies in extreme rainfall; during La Niña, however, precipitation increases due to moisture recirculation, which is limited by local potential evapotranspiration rates and hence less likely to produce extreme precipitation. Thus, our hypothesis of the nonlinear response mechanism would imply higher extreme rainfall anomalies during El Niño than

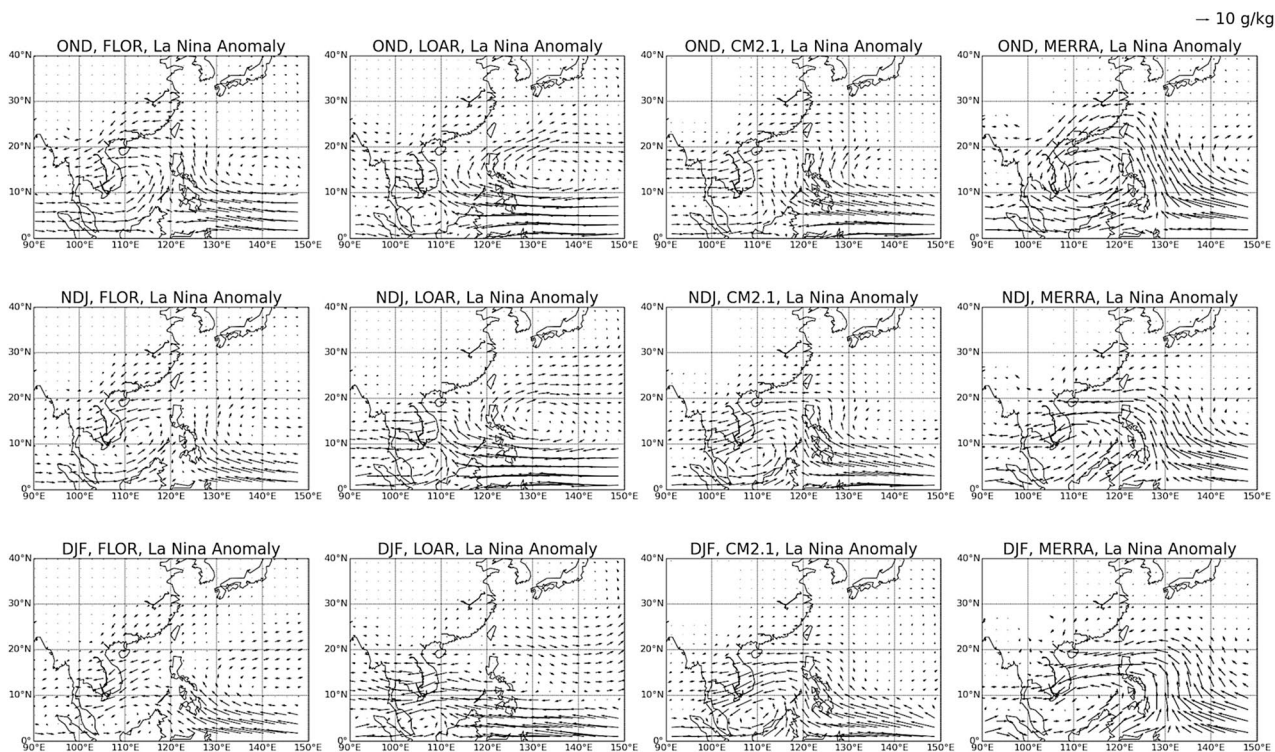


Fig. 12 As in Fig. 10, but for 850 hPa moisture flux anomalies during La Niña. Specific humidity and wind variables from MERRA are taken from the 3-h Assimilated Meteorological Fields simulation with $1.25^\circ \times 1.25^\circ$ horizontal resolution, for 1979–2014. During the fall/winter season, FLOR captures anomalous northeasterly moisture fluxes over the SEC region. The moisture flux anomalies are not captured in LOAR, and have an onshore component in CM2.1 so that the

mean P–E has a positive anomaly, but is not statistically significant. The moisture flux anomalies in MERRA (1979–2014) are also shown for comparison purposes; while we have discussed the moisture budget in the models, we have not done so for reanalysis products, since the evaporative flux exhibits a negligible response to La Niña in MERRA (not shown)

La Niña, and hence the difference between extreme and mean rainfall anomaly should be higher for El Niño than La Niña. As importantly, we do not rule out other possible reasons leading to the observed behavior of extreme rainfall during the ENSO phases.

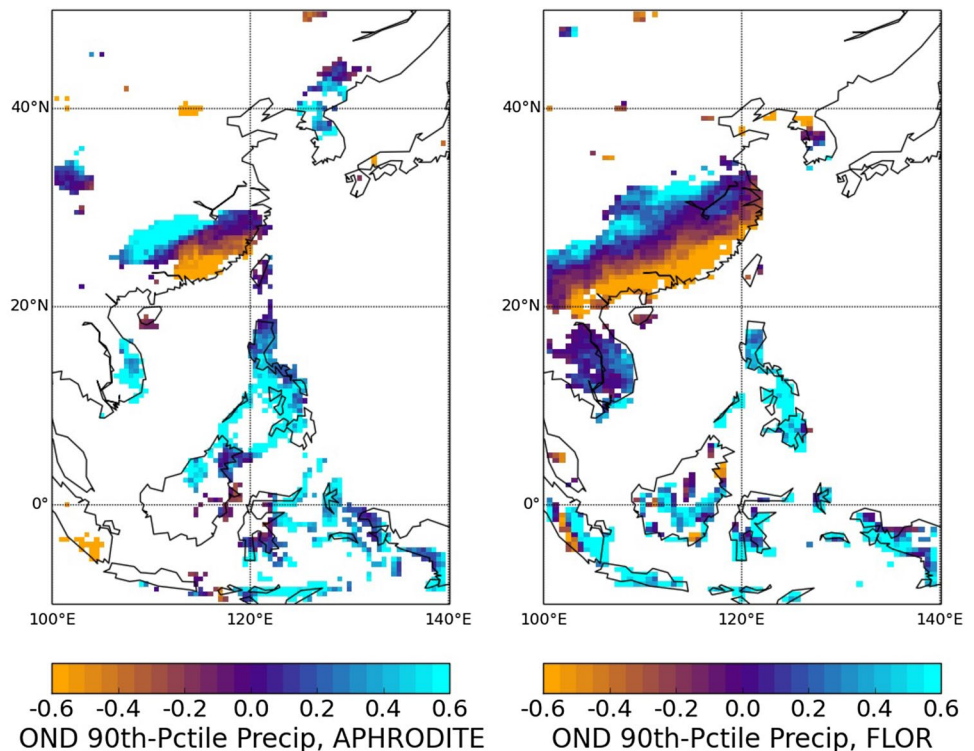
Our model hierarchy suggests that this behavior of extreme rainfall should be captured in the FLOR model but not in LOAR or CM2.1. In fact, not only does extreme rainfall (defined by the 90th percentile of seasonal rainfall) exhibit a nonlinear relationship in the APHRDITE observations and the FLOR model (Fig. 13), the extreme rainfall anomaly is also higher during El Niño than La Niña events (Fig. 14). The difference between these two anomalies during the OND season is better represented in observations than the FLOR model: while the mean rainfall anomaly is similar between La Niña and El Niño in FLOR and APHRDITE, the El Niño 90th percentile rainfall anomaly is 37.03% (80.86%) higher than the La Niña anomaly in FLOR (APHRDITE).

6 Conclusions

This study performs statistical diagnosis of a nonlinear rainfall response to ENSO along the coast of southeastern China, and provides an explanation of this nonlinearity based on the time evolution of macroscopic variables including precipitation, evaporation, soil moisture and the large-scale circulation. The findings of this study can be summarized as follows:

1. Higher mean rainfall is observed in the OND season during both El Niño and La Niña compared to the ENSO-Neutral phase, by approximately 0.4–0.5 mm/day on average per $^\circ\text{C}$ change. An index is developed from quasi-linear model fitting to quantify the nonlinearity of this rainfall response. The nonlinear signal is statistically significant at the 99% level, and is confirmed in other high-resolution observation datasets.

Fig. 13 Nonlinearity of OND extreme (90th percentile) rainfall response to ENSO, given by the linearity ratio L , in APHRODITE (left) and FLOR (right). Only locations whose anomalies are statistically significant at the one-sided 99% level are plotted



2. The nonlinearity in OND rainfall response to ENSO is captured in GFDL-FLOR model simulations in which sea-surface temperatures are restored to interannually varying observations, but not in the similarly nudged LOAR simulations, in which the nonlinear signal is closer to one-sided and noisier, nor in the CM2.1 model, in which no relationship is seen.
3. The El Niño results from the FLOR simulations are consistent with observational diagnostics in previous literature (Zhang et al. 1999; Wang et al. 2000), which suggested that the precipitation increases during El Niño are the result of anomalous onshore moisture fluxes. These moisture fluxes were in turn due to an anomalous high pressure to the north of the maritime continent. In contrast, LOAR and CM2.1 model the anomalous high westward, leading to anomalous fluxes with lower onshore components and noisier rainfall signals, and there is no significant El Niño rainfall response during OND in coastal southeastern China.
4. Positive rainfall anomalies during La Niña are driven by the persistence of terrestrial moisture availability in this region. We have established a diagnostic argument that during La Niña, anomalous precipitation minus evaporation ($P-E$) from the previous summer leads to anomalous soil moisture persisting to fall (in FLOR and LOAR, as seen in Fig. 11), during which precipitation and evaporation both increase through excess re-evaporation (the moisture recycling effect). Anomalous soil moisture is seen in the FLOR and LOAR models with more sophisticated land components (LM3), but not in CM2.1, which has a more primitive land component (LM2). Additionally, analysis of the moisture budget indicates that in both the FLOR and LOAR models, the relative contribution of moisture flux to precipitation is very small, compared to that of local evaporation, in the OND season. In other words, since the anomalous La Niña precipitation rate is very similar to that of evaporation in FLOR and LOAR, there is no room for non-local moisture fluxes to contribute to rainfall, and hence the moisture recycling effect. Correctly capturing the response of OND rainfall anomalies to ENSO requires sufficient sophistication in the model's land component to persist soil moisture anomalies across the seasons. The importance of land processes to the OND rainfall response to ENSO raises the possibility that changes in land-use and land-cover, and low-frequency changes in background soil moisture, due either to decadal climate variability or forced climate change, could affect the response of OND rainfall to La Niña over this region.
5. The fact that ENSO impacts rainfall nonlinearly through both the atmosphere component of the climate system and its interaction with land hydrology emphasizes the model hierarchy in which FLOR captures the nonlinear response through both a high atmospheric resolution and a more sophisticated land component, LOAR only captures the La Niña moisture recycling effect through the

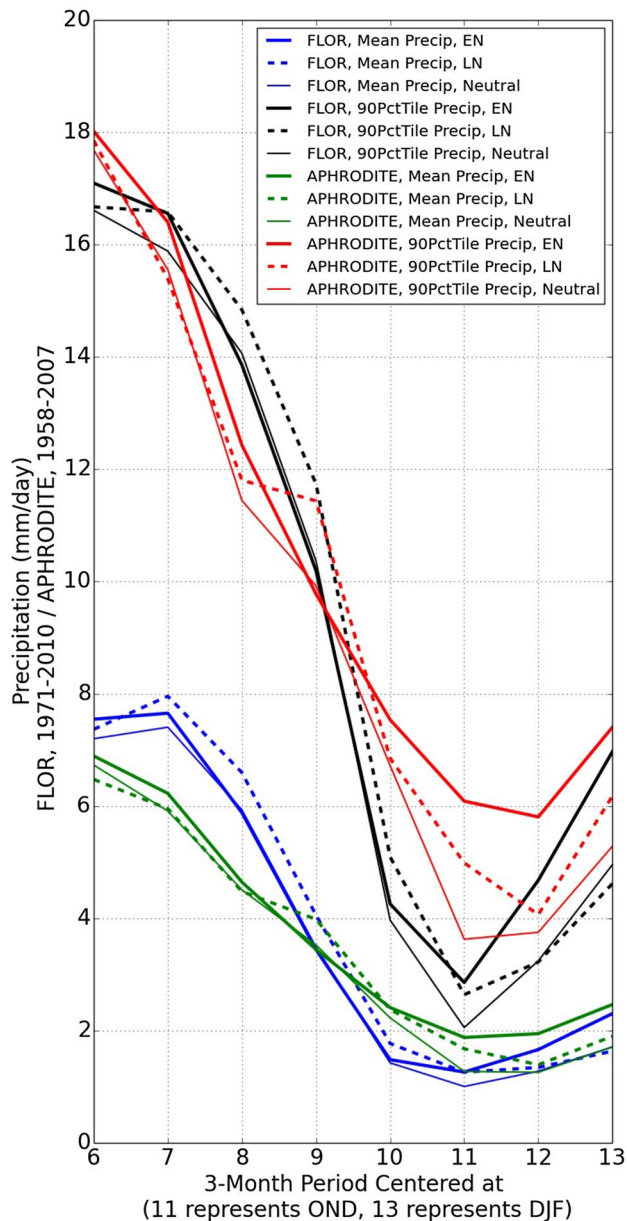


Fig. 14 Time evolution of seasonal mean and extreme (90th percentile) precipitation, in APHRODITE and FLOR, averaged over the SEC region (23°N–27°N, 111°E–118°E)

latter, while CM2.1 captures neither. The increased complexity of both the atmospheric and land components in FLOR over CM2.1 may serve to explain the improvement in forecast skill for FLOR seasonal forecast over CM2.1 (Jia et al. 2015), particularly over southeastern China.

- Extreme rainfall also behaves nonlinearly in coastal southeastern China, increasing during both ENSO phases. However, this nonlinear relationship is somewhat closer to one-sided, as opposed to the v-shaped response of seasonal-mean rainfall, becoming more

severe during El Niño than La Niña events. This asymmetry in the amplitude of the extreme rainfall increases between El Niño and La Niña reflect the contrasting impacts of the increases in anomalous moisture flux convergence during El Niño, which integrate evaporation over a large oceanic region, to the moisture recycling during La Niña, which is limited by local potential evapotranspiration rates.

Further testing of these hypothesis could be done, for example, by examining the processes of land-atmospheric interactions in the model components and parameterizations therein, and determining the types of land processes in LM3 that are most responsible for improving the La Niña response in FLOR and LOAR relative to CM2.1. Additionally, as shown in Figs. 10 and 12, the difference in anomalous circulation between reanalysis products (e.g. MERRA) and the GFDL models may also be the topic of further studies. Nevertheless, the main aim of this paper is to explore the robust nonlinear rainfall response to ENSO in several observational datasets and the FLOR model, which emphasizes the idea that while La Niña to first order can be approximated as the opposite to El Niño, nonlinearities in ENSO climatic impacts should also be taken into account, in an effort to improve seasonal predictions of climate. In light of the continued flooding risks associated with extreme weather and increasing population in the Pearl River Delta, it would be beneficial for these considerations to be included in future studies related to climate and climate change impacts in this region.

Acknowledgements The authors would like to thank Fanrong Zeng for conducting the CM2.1 simulations relevant for this study, and to Thomas Delworth and Will Cooke for the development of the LOAR model. This work is supported in part by National Oceanic and Atmospheric Administration (NOAA) Grants NA14OAR4830101 and NA14OAR4320106.

References

- Adler RF, Huffman GJ, Chang A, Ferraro R, Xie PP, Janowiak J, Rudolf B, Schneider U, Curtis S, Bolvin D, Gruber A (2003) The version-2 global precipitation climatology project (GPCP) monthly precipitation analysis (1979–present). *J Hydrometeorol* 4(6):1147–1167. [https://doi.org/10.1175/1525-7541\(2003\)004,1147:TVGPCP.2.0.CO;2](https://doi.org/10.1175/1525-7541(2003)004,1147:TVGPCP.2.0.CO;2)
- Alexander MA, Bladé I, Newman M, Lanzante JR, Lau NC, Scott JD (2002) The atmospheric bridge: the influence of ENSO teleconnections on air–sea interaction over the global oceans. *J Clim* 15(16):2205–2231
- An SI, Jin FF (2004) Nonlinearity and asymmetry of ENSO. *J Clim* 17(12):2399–2412. [https://doi.org/10.1175/1520-0442\(2004\)017<2399:NAAOE>2.0.CO;2](https://doi.org/10.1175/1520-0442(2004)017<2399:NAAOE>2.0.CO;2)
- Baldwin J, Vecchi G (2016) Influence of the Tian Shan on arid extratropical Asia. *J Clim* 29(16):5741–5762. <https://doi.org/10.1175/JCLI-D-15-0490.1>

- Barlow M, Nigam S, Berbery EH (2001) ENSO, Pacific decadal variability, and US summertime precipitation, drought, and stream flow. *J Clim* 14(9):2105–2128
- Cai W, Santoso A, Wang G, Yeh SW, An SI, Cobb KM, Collins M, Guilyardi E, Jin FF, Kug JS, Lengaigne M (2015) ENSO and greenhouse warming. *Nat Clim Change* 5:849–859. <https://doi.org/10.1038/nclimate2743>
- Chen M, Xie P, Janowiak JE, Arkin PA (2002) Global land precipitation: a 50-yr monthly analysis based on gauge observations. *J Hydrometeorol* 3(3):249–266
- Choi KY, Vecchi GA, Wittenberg AT (2013) ENSO transition, duration, and amplitude asymmetries: role of the nonlinear wind stress coupling in a conceptual model. *J Clim* 26(23):9462–9476. <https://doi.org/10.1175/JCLI-D-13-00045.1>
- Choi KY, Vecchi GA, Wittenberg AT (2015) Nonlinear zonal wind response to ENSO in the CMIP5 models: roles of the zonal and meridional shift of the ITCZ/SPCZ and the simulated climatological precipitation. *J Clim* 28(21):8556–8573. <https://doi.org/10.1175/JCLI-D-15-0211.1>
- Delworth TL, Broccoli AJ, Rosati A, Stouffer RJ, Balaji V, Beesley JA, Cooke WF, Dixon KW, Dunne J, Dunne KA, Durachta JW (2006) GFDL's CM2 global coupled climate models. Part I: formulation and simulation characteristics. *J Clim* 19(5):643–674. <https://doi.org/10.1175/JCLI3629.1>
- Delworth TL, Rosati A, Anderson W, Adcroft AJ, Balaji V, Benson R, Dixon K, Griffies SM, Lee HC, Pacanowski RC, Vecchi GA (2012) Simulated climate and climate change in the GFDL CM2.5 high-resolution coupled climate model. *J Clim* 25(8):2755–2781. <https://doi.org/10.1175/JCLI-D-11-00316.1>
- Dommenges D, Bayr T, Frauen C (2013) Analysis of the non-linearity in the pattern and time evolution of El Niño Southern Oscillation. *Clim Dyn* 40(11–12):2825–2847. <https://doi.org/10.1007/s00382-012-1475-0>
- Efron B, Tibshirani R (1985) The bootstrap method for assessing statistical accuracy. *Behaviormetrika* 12(17):1–35. https://doi.org/10.2333/bhmk.12.17_1
- Guo Z, Zhou T, Wu B (2017) The asymmetric effects of El Niño and La Niña on the East Asian winter monsoon and their simulation by CMIP5 atmospheric models. *J Meteorol Res* 31(1):82–93. <https://doi.org/10.1007/s13351-017-6095-5>
- Hoerling MP, Kumar A, Zhong M (1997) El Niño, La Niña, and the nonlinearity of their teleconnections. *J Clim* 10(8):1769–1786. [https://doi.org/10.1175/1520-0442\(1997\)010<1769:ENOLNA>2.0.CO;2](https://doi.org/10.1175/1520-0442(1997)010<1769:ENOLNA>2.0.CO;2)
- Hong CC, Li T, Chen YC (2010) Asymmetry of the Indian Ocean basinwide SST anomalies: roles of ENSO and IOD. *J Clim* 23(13):3563–3576. <https://doi.org/10.1175/2010JCLI3320.1>
- Jia L, Yang X, Vecchi GA, Gudgel RG, Delworth TL, Rosati A, Stern WF, Wittenberg AT, Krishnamurthy L, Zhang S, Msadek R (2015) Improved seasonal prediction of temperature and precipitation over land in a high-resolution GFDL climate model. *J Clim* 28(5):2044–2062. <https://doi.org/10.1175/JCLI-D-14-00112.1>
- Jin FF, An SI, Timmermann A, Zhao J (2003) Strong El Niño events and nonlinear dynamical heating. *Geophys Res Lett.* <https://doi.org/10.1029/2002GL016356>
- Kane RP (1997) Relationship of El Niño–Southern Oscillation and Pacific sea surface temperature with rainfall in various regions of the globe. *Mon Weather Rev* 125(8):1792–1800
- Lanzante JR (1996) Resistant, robust and non-parametric techniques for the analysis of climate data: theory and examples, including applications to historical radiosonde station data. *Int J Climatol* 16(11):1197–1226
- Larkin NK, Harrison DE (2002) ENSO warm (El Niño) and cold (La Niña) event life cycles: ocean surface anomaly patterns, their symmetries, asymmetries, and implications. *J Clim* 15(10):1118–1140. [https://doi.org/10.1175/1520-0442\(2002\)015,1118:EWENO.A.2.0.CO;2](https://doi.org/10.1175/1520-0442(2002)015,1118:EWENO.A.2.0.CO;2)
- Larkin NK, Harrison DE (2005) Global seasonal temperature and precipitation anomalies during El Niño autumn and winter. *Geophys Res Lett.* <https://doi.org/10.1029/2005GL022860>
- Lau NC, Nath MJ (2001) Impact of ENSO on SST variability in the North Pacific and North Atlantic: seasonal dependence and role of extratropical sea–air coupling. *J Clim* 14(13):2846–2866
- Lengaigne M, Vecchi GA (2010) Contrasting the termination of moderate and extreme El Niño events in coupled general circulation models. *Clim Dyn* 35(2–3):299–313. <https://doi.org/10.1007/s00382-009-0562-3>
- Li J, Fan K, Xu Z (2016) Asymmetric response in Northeast Asia of summer NDVI to the preceding ENSO cycle. *Clim Dyn* 47(9–10):2765–2783. <https://doi.org/10.1007/s00382-016-2996-8>
- Muñoz ÁG, Yang X, Vecchi GA, Robertson AW, Cooke WF (2017) A weather-type-based cross-time-scale diagnostic framework for coupled circulation models. *J Clim* 30(22):8951–8972
- Murakami H, Vecchi GA, Underwood S, Delworth TL, Wittenberg AT, Anderson WG, Chen JH, Gudgel RG, Harris LM, Lin SJ, Zeng F (2015) Simulation and prediction of category 4 and 5 hurricanes in the high-resolution GFDL HiFLOR coupled climate model. *J Clim* 28(23):9058–9079. <https://doi.org/10.1175/JCLI-D-15-0216.1>
- Ohba M, Ueda H (2009) Role of nonlinear atmospheric response to SST on the asymmetric transition process of ENSO. *J Clim* 22(1):177–192. <https://doi.org/10.1175/2008JCLI2334.1>
- Rasmusson EM, Carpenter TH (1982) Variations in tropical sea surface temperature and surface wind fields associated with the Southern Oscillation/El Niño. *Mon Weather Rev* 110(5):354–384. [https://doi.org/10.1175/1520-0493\(1982\)110<0354:VITSST>2.0.CO;2](https://doi.org/10.1175/1520-0493(1982)110<0354:VITSST>2.0.CO;2)
- Rayner NA, Parker DE, Horton EB, Folland CK, Alexander LV, Rowell DP, Kent EC, Kaplan A (2003) Global analyses of sea surface temperature, sea ice, and night marine air temperature since the late nineteenth century. *J Geophys Res Atmos* 108(D14):4407. <https://doi.org/10.1029/2002JD002670>
- Ropelewski CF, Halpert MS (1987) Global and regional scale precipitation patterns associated with the El Niño/Southern Oscillation. *Mon Weather Rev* 115(8):1606–1626
- Seager R, Vecchi GA (2010) Greenhouse warming and the 21st century hydroclimate of southwestern North America. *Proc Natl Acad Sci* 107(50):21277–21282. <https://doi.org/10.1073/pnas.0910856107>
- Smith TM, Reynolds RW, Peterson TC, Lawrimore J (2008) Improvements to NOAA's historical merged land–ocean surface temperature analysis (1880–2006). *J Clim* 21(10):2283–2296. <https://doi.org/10.1175/2007JCLI2100.1>
- Tong J, Qiang Z, Deming Z, Yijin W (2006) Yangtze floods and droughts (China) and teleconnections with ENSO activities (1470–2003). *Quat Int* 144(1):29–37
- van der Wiel K, Kapnick SB, Vecchi GA, Cooke WF, Delworth TL, Jia L, Murakami H, Underwood S, Zeng F (2016) The resolution dependence of contiguous US precipitation extremes in response to CO₂ forcing. *J Clim* 29(22):7991–8012. <https://doi.org/10.1175/JCLI-D-16-0307.1>
- Vecchi GA (2006) The termination of the 1997–98 El Niño. Part II: mechanisms of atmospheric change. *J Clim* 19(12):2647–2664
- Vecchi GA, Harrison DE (2006) The termination of the 1997–98 El Niño. Part I: mechanisms of oceanic change. *J Clim* 19(12):2633–2646
- Vecchi GA, Delworth T, Gudgel R, Kapnick S, Rosati A, Wittenberg AT, Zeng F, Anderson W, Balaji V, Dixon K, Jia L (2014) On the seasonal forecasting of regional tropical cyclone activity. *J Clim* 27(21):7994–8016. <https://doi.org/10.1175/JCLI-D-14-00158.1>
- Wang B, Wu R, Fu X (2000) Pacific–East Asian teleconnection: how does ENSO affect East Asian climate? *J Clim* 13(9):1517–1536

- Willmott CJ, Matsuura K (2001) Terrestrial air temperature and precipitation: monthly and annual time series (1950–1999). Center for Climate Research, Version 1. http://climate.geog.udel.edu/~climate/html_pages/README_ghcn_ts2.html
- Wu R, Hu ZZ, Kirtman BP (2003) Evolution of ENSO-related rainfall anomalies in East Asia. *J Clim* 16(22):3742–3758
- Xie P, Arkin PA (1997) Global precipitation: a 17-year monthly analysis based on gauge observations, satellite estimates, and numerical model outputs. *Bull Am Meteor Soc* 78(11):2539–2558
- Yatagai A, Arakawa O, Kamiguchi K, Kawamoto H, Nodzu MI, Hamada A (2009) A 44-year daily gridded precipitation dataset for Asia based on a dense network of rain gauges. *SOLA* 5:137–140. <https://doi.org/10.2151/sola.2009-035>
- Yatagai A, Kamiguchi K, Arakawa O, Hamada A, Yasutomi N, Kito A (2012) APHRODITE: constructing a long-term daily gridded precipitation dataset for Asia based on a dense network of rain gauges. *Bull Am Meteor Soc* 93(9):1401–1415. <https://doi.org/10.1175/BAMS-D-11-00122.1>
- Zebiak SE, Orlove B, Muñoz ÁG, Vaughan C, Hansen J, Troy T, Thomson MC, Lustig A, Garvin S (2015) Investigating El Niño–Southern Oscillation and society relationships. *Wiley Interdiscip Rev Clim Change* 6(1):17–34. <https://doi.org/10.1002/wcc.294>
- Zhang R, Sumi A (2002) Moisture circulation over East Asia during El Niño episode in northern winter, spring and autumn. *J Meteorol Soc Japan Ser II* 80(2):213–227
- Zhang R, Sumi A, Kimoto M (1999) A diagnostic study of the impact of El Niño on the precipitation in China. *Adv Atmos Sci* 16(2):229–241
- Zhang T, Perlwitz J, Hoerling MP (2014) What is responsible for the strong observed asymmetry in teleconnections between El Niño and La Niña? *Geophys Res Lett* 41(3):1019–1025. <https://doi.org/10.1002/2013GL058964>